Enrichment of calcium in sea spray aerosol: Insights from bulk measurements and individual particle analysis during the R/V *Xuelong* cruise in the summertime Ross Sea, Antarctica

Bojiang Su [a, b], Xinhui Bi [a, c], Zhou Zhang [b, d], Yue Liang [e], Congbo Song [f], Tao Wang [a, b], Yaohao Hu [a, b], Lei Li [g, *], Zhen Zhou [g], Jinpei Yan [h], Xinming Wang [a, c], Guohua Zhang [a, c, *]

[a] State Key Laboratory of Organic Geochemistry and Guangdong Provincial Key Laboratory of Environmental Protection and Resources Utilization, Guangzhou Institute of Geochemistry, Chinese Academy of Sciences, Guangzhou 510640, China

[b] University of Chinese Academy of Sciences, Beijing 100049, China

[c] Guangdong-Hong Kong-Macao Joint Laboratory for Environmental Pollution and Control, Guangzhou 510640, China

[d] State Key Laboratory of Isotope Geochemistry, Guangzhou Institute of Geochemistry, Chinese Academy of Sciences, Guangzhou 510640, China

[e] Department of Civil and Environmental Engineering, Faculty of Science and Technology, University of Macau, Taipa, Macau, China

[f] National Centre for Atmospheric Science (NCAS), University of Manchester, Manchester M13 9PL, UK

[g] Institute of Mass Spectrometry and Atmospheric Environment, Jinan University, Guangzhou 510632, China

[h] Key Laboratory of Global Change and Marine Atmospheric Chemistry, Third Institute of Oceanography, Ministry of Natural Resources, Xiamen 361005, China

*Corresponding author: zhanggh@gig.ac.cn; lileishdx@163.com

Abstract: Although calcium is known to be enriched in sea spray aerosols (SSAs), the factors that affect its enrichment remain ambiguous. In this study, we examine how environmental factors affect the distribution of water-soluble calcium (Ca^{2+}) distribution in SSAs. We obtained our dataset from observations taken during a research cruise on the R/V *Xuelong* cruise in the Ross Sea, Antarctica, from December 2017 to February 2018. Our observations showed that the enrichment of Ca^{2+} in aerosol samples was enhanced under specific conditions, including lower temperatures (< -3.5 ℃), lower wind speeds (< 7 m s^{-1}), and the presence of sea ice. Our analysis of individual particle mass spectra revealed that a significant portion of calcium in SSAs was likely bound with organic matter (in the form of a single-particle type, OC-Ca). Our findings suggest that current estimations of Ca^{2+} enrichment based solely on water-soluble Ca^{2+} may be inaccurate. Our study is the first to observe a single-particle type dominated by calcium in the Antarctic atmosphere. Our findings suggest that future Antarctic atmospheric modeling should take into account the environmental behavior of individual OC-Ca. With the ongoing global warming and retreat of sea ice, it is essential to understand the mechanisms of calcium enrichment and the mixing state of individual particles to better comprehend the interactions between aerosols, clouds, and climate during the Antarctica summer.

Key points:

- Ca^{2+} enrichment in sea spray aerosols (SSAs) was observed at lower ambient temperatures, lower wind speeds, and in the presence of sea ice.
- Individual particle analysis revealed a significant portion of internally mixed organics with calcium particles in the Antarctic summer atmosphere.
- Current water-soluble estimation of Ca^{2+} enrichment in SSAs may be inaccurate without considering organically complexed calcium.

Keywords:

Sea spray aerosol; Calcium enrichment; Individual particle analysis; Environmental factors; Internally mixed organics with calcium particles; Antarctic summer atmosphere.

1 Introduction

Sea spray aerosols (SSAs) govern radiative forcing by directly scattering and absorbing solar radiation over the remote ocean (Murphy et al., 1998), and they affect the microphysical properties of marine clouds by serving as cloud condensation nuclei (CCN) and ice nuclei (IN) (Wilson et al., 2015; Brooks and Thornton, 2018; Willis et al., 2018). Calcium is one of the components of SSA, which can present as inorganic calcium (e.g., $CaCl_2$ and $CaSO_4$) (Chi et al., 2015) as well as organic calcium (i.e., Ca^{2+} can readily induce the gelation of organic matter, presenting as the most efficient gelling agent) (Carter-Fenk et al., 2021). Calcium enrichment and chemical signature can affect some physicochemical properties of SSAs such as alkalinity and hygroscopicity (Salter et al., 2016; Mukherjee et al., 2020), which is critical for understanding aerosol-cloud interactions over the remote marine boundary layer (Keene et al., 2007; Leck and Svensson, 2015; Bertram et al., 2018).

Several studies have demonstrated significant enrichment of calcium (Ca^{2+}) in SSAs compared to bulk seawater, as briefly summarized in **Table S1** and documented by Keene et al. (2007), Hara et al. (2012), Cochran et al. (2016), Salter et al. (2016), Cravigan et al. (2020), and Mukherjee et al. (2020). For example, Hara et al. (2012) found that the Ca^{2+} enrichment of aerosol samples was sensitive to sea salt fractionation during the cold winter-spring season over the Antarctic coast. Leck and Svensson (2015) suggested that Ca^{2+} enrichment in SSAs is attributed to bubble bursts on sea ice leads over the Arctic area. Similarly, low wind-driven bubble bursts were regarded as a major reason for the Ca^{2+} enrichment in SSAs during an Arctic cruise (Mukherjee et al., 2020). These results shed light on the Ca^{2+} enrichment process; however, our understanding of how environmental factors synergistically affect such enrichment processes remains unclear.

To date, a unified consensus on the chemical form of calcium to explain calcium enrichment in SSAs has not been reached. Two hypotheses have been proposed: (i) Calcium enrichment is dominated by inorganic calcium, such as $CaCO_3$ and $CaCl_2$. Ca^{2+} is enriched close to the seawater surface in the form of ionic clusters (most probably with carbonate ions) (Salter et al., 2016). Another source of $CaCO_3$ is directly from calcareous shell debris (Keene et al., 2007). Through bubble bursts, both $CaCO_3$ and $CaCl_2$ along with sea salt can be emitted into the atmosphere. In addition, the sea salt fractionation by precipitation of ikaite ($CaCO_3 \cdot 6H_2O$) may contribute to calcium enrichment in aerosol during the freezing of sea ice (Hara et al., 2012). (ii) Calcium enrichment is attributed to organically complexed calcium. Ca^{2+} may bind with organic matter, which is relevant with marine microgels and/or coccolithophore phytoplankton scales, and can be emitted by bubble bursting (Oppo et al., 1999; Sievering, 2004; Leck and Svensson, 2015; Cochran et al., 2016; Kirpes et al., 2019; Mukherjee et al., 2020). The chemical form of calcium can determine its atmospheric role. Inorganic calcium may exhibit stronger aerosol alkalinity and hygroscopicity than organic calcium (Salter et al., 2016; Mukherjee et al., 2020). However, current estimations of calcium enrichment based solely on water-soluble Ca^{2+} may not precisely explain the calcium distribution in SSAs. This is because the amount of low water-soluble complexation of Ca^{2+} with organic matter (e.g., aged Ca^{2+}-assembled gel-like particles) (Orellana and Verdugo, 2003; Leck and Bigg, 2010; Russell et al., 2010; Orellana et al., 2011; Leck and Svensson, 2015) and insoluble Ca^{2+} in the form of calcareous shell debris or the like may not be considered. Thus, an alternative method, such as discerning the mixing state based on single-particle analysis, may provide unique insights into the chemical form of calcium, and thus the mechanisms of calcium enrichment in SSAs.

As a part of the 34th Chinese Antarctic Research Expedition (CHINARE ANT34th), this study aimed to investigate the influencing factors and possible mechanisms of calcium enrichment in SSAs through R/V *Xuelong* cruise observation campaigns over the Ross Sea, Antarctica. An in-situ gas and aerosol composition monitoring system (IGAC) was employed to determine the extent of Ca^{2+} enrichment in SSAs. Single-particle aerosol mass spectrometry (SPAMS) was utilized to measure the size and chemical signature (i.e., mixing state) of individual calcareous particles. We first investigated the impact of environmental factors such as ambient temperature, wind speed, sea ice fraction, chlorophyll-a concentration, and back trajectory coverage on Ca^{2+} enrichment in SSAs. Then, the mechanisms of calcium enrichment in SSAs were inferred according to the mixing state of individual calcareous particles.

2 Methodology

2.1 The R/V *Xuelong* cruise and observation regions

Our study focused on the Ross Sea region of Antarctica (50 to 78° S, 160 to 185° E) (**Fig. 1**), where we conducted two separate observation campaigns aboard the R/V *Xuelong*. During the observations, this region was relatively isolated from the impact of long-range transport of anthropogenic aerosols and has experienced the sea ice retreat (Yan et al., 2020a).

The first observation campaign (Leg I) took place from December 2-20, 2017, during the sea ice period. The second campaign (Leg II) was conducted from January 13 to February 14, 2018, during the period without sea ice. The sampling design for Leg I and Leg II aimed to investigate how changing environmental factors affect the enrichment extent of calcium and the characteristics of individual particles.

115 **2.2 Meteorological parameters and satellite data of air masses, sea ice, and chlorophyll-a**

116 We measured various meteorological parameters, such as ambient temperature, relative
117 humidity (RH), wind speed, and true wind direction using an automated meteorological station
118 located on the top deck of the R/V *Xuelong* (**Fig. S1 and Table S2**).

119 To determine the type of air masses, we first overviewed the 72-hour back trajectory with
120 daily resolution per each starting location by using the NOAA Hybrid Single-Particle Lagrangian
121 Integrated Trajectories (HYSPLIT, version 4.9) model (**Fig. S2**). Additionally, we conducted a 96-
122 hour back trajectory analysis with an hourly resolution, which covered the enhanced calcium
123 enrichment events associated with sea ice fraction and chlorophyll-a concentration (discussed in
124 section 3.1), using the TrajStat in Meteoinfo (version 3.5.8) (Wang et al., 2009; Wang, 2014).
125 Meteorological data used for back trajectory analysis obtained from the Global Data Assimilation
126 System (GDAS, ftp://ftp.arl.noaa.gov/pub/archives). Moreover, we obtained the monthly sea ice
127 fraction from the Sea Ice Concentration Climate Data Record with a spatial resolution of 25 km
128 (https://www.ncei.noaa.gov/products/climate-data-records/sea-ice-concentration) and the 8-day
129 chlorophyll-a concentration from MODIS-aqua with a spatial resolution of 4 km
130 (https://modis.gsfc.nasa.gov) (**Fig. S3**).

131 During the R/V *Xuelong* cruise observation campaigns, leg I was dominantly affected by the
132 air masses from the sea ice-covered open water (92%, by trajectory coverage), and leg II was
133 mainly affected by the air masses from continental Antarctica (58%) (**Table S2**). The average
134 ambient temperature (-4.0 ± 1.4 ℃ vs. -3.1 ± 2.2 ℃), wind speed (7.2 ± 5.5 m s^{-1} vs. 7.1 ± 4.2 m
135 s^{-1}), and chlorophyll-a concentration (0.51 ± 0.29 μg L^{-1} vs. 0.44 ± 0.18 μg L^{-1}) varied slightly
136 between legs I and II (**Table S2**).

2.3 Contamination control during observation campaigns

During the research cruise, the major contamination source was identified as emissions from a chimney located at the stern of the vessel and about 25 m above the sea surface. To mitigate the potential impact of ship emissions on aerosol sampling, we have taken several measures. Firstly, a total suspended particulate (TSP) sampling inlet connecting to the monitoring instruments was fixed to a mast 20 m above the sea surface, located at the bow of the vessel. In addition, the sampling inlet was fixed on a ship pillar with a rain cover, which could minimize the potential influence of violent shaking of the ship and sea waves. Secondly, sampling was only conducted while the ship was sailing, to avoid the possible effect of ship emission on aerosol sampling under the low diffusion condition. Lastly, we did not observe the mass spectral characteristics associated with ship emission (e.g., particles simultaneously contain *m/z* 51 $[V]^+$, 67 $[VO]^+$, and element carbon) during the observation campaigns (Liu et al., 2017; Passig et al., 2021). These measures ensured that the collected data were representative and reliable for subsequent analysis.

2.4 Instrumentation

An IGAC (Model S-611, Machine Shop, Fortelice International Co. Ltd., Taiwan, China) and a SPAMS (Hexin Analytical Instrument Co., Ltd., China) were synchronously employed to determine water-soluble ion mass concentrations of bulk aerosol and the size and chemical composition of individual particles in real-time with hourly resolution (**Figs. 2** and **S4**). In the aerosol sampling procedure, a TSP inlet with a PM_{10} cyclone (trap efficiency greater than 99% for particles > 0.3 μm, D_{a50} = 10 ± 0.5 μm) was used for IGAC sampling and a $PM_{2.5}$ cyclone (D_{a50} = 2.5 ± 0.2 μm) to remove particles larger than 2.5 μm for SPAMS. All instruments were connected

158 using conductive silicon tubing with an inner diameter of 1.0 cm.

159 **2.4.1 Aerosol water-soluble ion constituents**

160 The details of the analytical method of IGAC have been described in previous studies (Young
161 et al., 2016; Yan et al., 2019; Yan et al., 2020b). Briefly, the IGAC system consisted of three main
162 units, including a Wet Annular Denuder (WAD), a Scrub and Impact Aerosol Collector (SIAC),
163 and an ion chromatograph (IC, Dionex ICS-3000) (**Fig. 2**). Gases and aerosols were passed
164 through WAD with a sampling flow of 16.7 L min^{-1}. Two concentric Pyrex glass cylinders with a
165 length of 50 cm and inner and outer diameters of 1.8 and 2.44 cm were assembled to WAD, in
166 which the inner walls of the annulus were wetted with ultrapure water (18.2 MΩ cm^{-1}). This part
167 was responsible for the collection of acidic and basic gases by diffusion and absorption of a
168 downward-flowing aqueous solution. The SIAC had a length of 23 cm and a diameter of 4.75 cm,
169 which was positioned at an angle to facilitate the collection of enlarged particles. The collected
170 particles were separated firstly, continually enlarged by vapor steam, and then accelerated through
171 a conical-shaped impaction nozzle and collected on an impaction plate. Each aerosol sample was
172 collected for 55 minutes and injected for 5 minutes. The injection loop size was 500 μL for both
173 anions and cations, which were subsequently analyzed by IC. The collection efficiency of aerosol
174 and gas samples before they entered IC was previously reported higher than 89% (for 0.056 μm
175 particles, 89%; for 1 μm particles, 98%; for gas samples, > 90%) (Chang et al., 2007; Tian et al.,
176 2017). The target ion concentrations were calibrated with a coefficient of determination (r^2) above
177 0.99 by using standard solutions (0.1-2000 μg L^{-1}). The detection limits for Na, Cl, Ca, K, and Mg
178 were 0.03, 0.03, 0.019, 0.011, and 0.042 μg L^{-1} (aqueous solution), respectively. The systematic

error of the IC systems was generally less than 5%. The detection limits for Na^+, Cl^-, Ca^{2+}, K^+, and Mg^{2+} were 0.03, 0.03, 0.019, 0.011, and 0.042 μg L^{-1} (aqueous solution), respectively.

Throughout the observation campaigns, the mean Na^+ and Ca^{2+} mass concentrations were 364.64 ng m^{-3} (ranging from 6.66 to 4580.10 ng m^{-3}) and 21.20 ng m^{-3} (ranging from 0.27 to 334.40 ng m^{-3}), respectively, which were 10 times higher than the detection limits. Analytical uncertainty of Ca^{2+} enrichment based on water-soluble analysis was estimated at less than 11% (**Supporting Information, SI text S1**).

It should be clarified that the water-soluble ion mass concentration included the pure inorganic part (e.g., pure sea salt, NaCl) and mixed organic-inorganic part (e.g., gel-like particles) (Quinn et al., 2015). Numerous studies have reported that primary SSAs exhibited moderate hygroscopicity and water solubility due to a certain water-soluble organic fraction (~ 25%, by mass), such as carboxylates, lipopolysaccharides (LPSs), humic substances, and galactose (Oppo et al., 1999; Quinn et al., 2015; Schill et al., 2015; Cochran et al., 2017). For example, Oppo et al. (1999) indicated that humic substances were an important pool of water-soluble natural surfactants (40-60%) in marine surfactant organic matter. In addition, LPSs are preferentially transferred to submicron SSAs during bubble bursting and exhibit a certain solubility of 5 g L^{-1} in pure water. (Facchini et al., 2008; Schill et al., 2015). Therefore, both organic and inorganic parts with a water-soluble nature could be retained, contributing to the water-soluble ion mass concentration (e.g., Ca^{2+}).

2.4.2 Single-particle analysis

A brief description of SPAMS has been provided elsewhere (Li et al., 2011). Briefly, the

aerosols were drawn into SPAMS by a $PM_{2.5}$ inlet after a silica gel dryer (**Fig. 2**). A collimated particle beam focused by an aerodynamic lens was then accelerated in an accelerating electric field and passed through two continuous laser beams (Nd: YAG laser, 532 nm). The obtained time of flight (TOF) and velocity of individual particles were used to calculate the vacuum aerodynamic diameter (D_{va}) based on a calibration curve. Subsequently, particles with a specific velocity were desorbed and ionized by triggering a pulse laser (an Nd: YAG laser, 266 nm, 0.6 ± 0.06 mJ was used in this study). The ion fragments were recorded using a bio-polar TOF mass spectrometer. Before the use of SPAMS, standard polystyrene latex spheres (0.2-2 μm, Duke Scientific Corp., Palo Alto, CA) and $PbCl_2$ and $NaNO_3$ (0.35 μm, Sigma-Aldrich) solutions were used for the size and mass spectral calibration, respectively. The hit rate, defined as the ratio of ionized particles to all sampled particles, of the SPAMS was ~ 11% during the cruise observation campaigns.

During the R/V *Xuelong* cruise observation campaigns, approximately 930,000 particles with mass spectral fingerprints and D_{va} ranging from 0.2 to 2 μm were measured. An adaptive resonance theory neural network (ART-2a) was used to group the particles into several clusters based on their mass spectral fingerprints, using parameters of a vigilance factor of 0.85, a learning rate of 0.05, and a maximum of 20 iterations (Song and Hopke, 1999). The manually obtained clusters were sea salt (SS, 16.5%), aged sea salt (SS-aged, 8.1%), sea salt with biogenic organic matter (SS-Bio, 3.1%), internally mixed organics with calcium (OC-Ca, 48.7%), internally mixed organics with potassium (OC-K, 13.7%), organic-carbon-dominated (OC, 7.0%), and element carbon (EC, 2.9%) (**Fig. S5 and Table S3**) (Prather et al., 2013; Collins et al., 2014; Su et al., 2021). All single-particle types had marine origins with typical mass spectral characteristics of Na

(*m/z* 23), Mg (*m/z* 24), K (*m/z* 39), Ca (*m/z* 40), and Cl (*m/z* -35 and -37), except for EC (**SI text S2**). There was little difference in individual particle analysis regarding chemical composition, size, and mixing state of particle clusters obtained from leg I and leg II (**SI Text S3**).

3 Results

3.1 Ca^{2+} enrichment dominated by environmental factors

We propose that both Na^+ and Ca^{2+} in our observations originated from marine sources. The mass concentration of Na^+ exhibited a strong positive correlation with that of Cl^- ($r = 0.99$, $p < 0.001$) and Mg^{2+} ($r = 0.99$, $p < 0.001$) (**Fig. S6**), indicating that they had a common origin (i.e., sea spray). However, it is not surprising that the mass concentration of Na^+ showed a relatively weak correlation with that of Ca^{2+} ($r = 0.51$, $p < 0.001$) (**Fig. S6**). This can be explained by the low water-soluble complexation of Ca^{2+} with organic matter and/or insoluble Ca^{2+} in the form of calcareous shell debris, such as $CaCO_3$. In addition, the potential impact of long-range transport of anthropogenic aerosols and dust contributing to Ca^{2+} may be limited due to the predominance of polar air masses during the observation campaigns (**Fig. S2**).

The enrichment factor (EF*x*), defined as the mass concentration ratio of a specific species *X* to Na^+ in aerosols to that in bulk seawater, is generally used to describe the enrichment extent of species *X* in aerosols.

$$EFx = \frac{([X]/[Na^+])_{aerosol}}{([X]/[Na^+])_{seawater}}$$

An EF*x* > 1 indicates a positive enrichment; otherwise, it indicates depletion. Generally, the ratio of Ca^{2+} to Na^+ in seawater is 0.038 (w/w) (Boreddy and Kawamura, 2015; Su et al., 2022). During the whole cruise, the hourly average EF_{Ca} was 2.76 ± 6.27 (mean ± standard deviation (M

± SD), n = 1051, ranged from 0.01 to 85, median =1.18, interquartile range (IQR) = 1.85). Similar to previous studies (Salter et al., 2016), positive magnesium (Mg^{2+}) and potassium (K^{+}) enrichment in SSAs was also observed (**SI text S4**).

Figure 3 presents the enrichment factor of Ca^{2+} (EF_{Ca}) at different ambient temperatures (separated by a mean value of -3.5 ℃), wind speeds (separated by a mean value of 7 m s^{-1}), and in the presence/absence of sea ice during the entire observation campaign. The results indicated that the highest EF_{Ca} zone (M ± SD = 3.83 ± 3.43, median = 2.66, IQR = 3.37, n = 144) occurred at a lower ambient temperature (< -3.5 ℃), lower wind speed (< 7 m s^{-1}) and in the presence of sea ice (**Fig. 3d**). Compared to the contrary conditions (i.e., ambient temperatures ≥ -3.5 ℃, wind speeds ≥ 7 m s^{-1}, and the absence of no sea ice), there was almost calcium depletion (EF_{Ca}, M ± SD = 1.01 ± 0.80, median = 0.70, IQR = 0.73, n = 182) (**Fig. 3c**). Notably, we observed a higher EF_{Ca} during the sea ice period than during the period without sea ice (3.83 ± 3.43 vs. 2.45 ± 3.09 by M ± SD and 2.66 vs. 1.18, by median) (**Fig. 3d**), under the conditions of ambient temperatures < -3.5 ℃ and wind speeds < 7 m s^{-1}. In addition, we also observed more frequent Ca^{2+} enrichment events during the sea ice period (71.0% in leg I) compared to the period without sea ice (47.7% in leg II) (**Table S2**). Moreover, the increased EF_{Ca} varied with decreasing ambient temperature and wind speed and with increasing sea ice fraction, as shown in **Fig. 4**. Taken together, our results indicate that the enhanced Ca^{2+} enrichment in SSAs is sensitive to the lower temperature, lower wind speeds, and the presence of sea ice.

We further analyzed the distribution of Ca^{2+} enrichment concerning 96-hour back trajectories with sea ice fraction and chlorophyll-a concentration, as shown in **Fig. 5**. During the observation campaigns, we identified five areas with continuous enhancement of Ca^{2+} enrichment, namely,

Area 1 and 2 during the leg II, and Area 3,4, and 5 during the leg I. Our results indicated that air masses traveling over the sea ice and marginal ice zone (> 95%, by trajectory coverage) in Areas 3, 4, and 5, as well as those over the sea ice (28%-33%) and land-based Antarctic ice (57-59%) in Area 1 and 2, were strongly associated with the increased calcium enrichment (**Table S4**). These pieces of evidence further support the influence of sea ice on the increased calcium enrichment, while simultaneously ruling out the influence of long-range transport of anthropogenic aerosol and dust outside the Antarctic.

We observed that a series of high EF_{Ca} cases in Area 1 were associated with a high concentration of chlorophyll-a (0.99 ± 1.65 μg L^{-1}). However, it is unlikely that phytoplankton and/or bacteria are responsible for the enhanced EF_{Ca} cases due to the weak correlation ($r = 0.12$, $p < 0.01$) between the chlorophyll-a concentration and EF_{Ca} values (**Fig. S7**). Moreover, although the ship track of leg II covered large areas with high chlorophyll-a concentrations, the high EF_{Ca} values were only present at the narrow temporal and spatial scales. Furthermore, results from back trajectories indicated that air masses did not significantly travel through the region with elevated chlorophyll-a concentration. Therefore, we suggest that the impact of chlorophyll-a concentration on Ca^{2+} enrichment may be limited.

3.2 Single-particle characteristics of Ca-containing particles

To elucidate the mixing state of individual calcareous particles, we set a threshold of *m/z* 40 $[Ca]^+$ to reclassify all single-particle types that were obtained from the ART-2a algorithm. This means that all reclassified particles contain signals of *m/z* 40 $[Ca]^+$. A total of ~ 580, 000 Ca-containing particles were distributed among all particle types, accounting for ~ 62% of the total

obtained particles. OC-Ca was the dominant (~ 72%, by occurrence frequency) particle type among all Ca-containing particles, followed by SS-Ca (calcium-containing sea salt, ~ 12%) (**Fig. 6h**). Each of the remaining particle types accounted for negligible fractions (< 7%) in the total of Ca-containing particles, and were classified as "Other". Thus, they were not included in the following discussion.

OC-Ca was characterized by a prominent ion signature for *m/z* at 40 $[Ca]^+$ in the positive mass spectrum and organic marker ions of biological origin (e.g., organic nitrogen, phosphate, carbohydrate, siliceous materials, and organic carbon) in the negative spectrum (**Fig. 6d**). Specifically, organic nitrogen (*m/z* -26 $[CN]^-$ and -42 $[CNO]^-$) showed the largest number fraction (NF) at ~88% (**Fig. S5h**), which is likely derived from organic nitrogen species, such as amines amino groups, and/or cellulose (Czerwieniec et al., 2005; Srivastava et al., 2005; Köllner et al., 2017; Dall'osto et al., 2019). Higher NFs of phosphate (16%; *m/z* -63 $[PO_2]^-$ and -79 $[PO_3]^-$), carbohydrates (24%; *m/z* -45 $[CHO_2]^-$, -59 $[C_2H_3O_2]^-$, and -73 $[C_3H_5O_2]^-$), siliceous materials (40%; *m/z* -60 $[SiO_2]^-$), and organic carbon (37%; *m/z* 27 $[C_2H_3]^-$ and 43 $[C_2H_3O_3]^-$) were also observed in OC-Ca relative to other particle types (**Fig. S5h**). These organic ion signatures likely correspond to phospholipids, mono- and polysaccharides, and biosilica structures (e.g., exoskeletons or frustules), which may be derived from the intact heterotrophic cells, fragments of cells, and exudates of phytoplankton and/or bacterial (Prather et al., 2013; Guasco et al., 2014; Zhang et al., 2018). Besides, the strong organic ion intensities may truly reflect the amount of organic material in OC-Ca, because the particles are sufficiently dry during the ionization process (i.e., complete positive and negative mass spectra) (Gross et al., 2000). Notably, the possible ion signals of bromide (*m/z* -79 and -81) were observed in OC-Ca, indicating a potential source of

blowing snow (Yang et al., 2008; Song et al., 2022).

The OC-Ca particles are most likely classified as a distinct SSA population, probably of marine biogenic origin. Sea salt particles typically exhibit a stronger *m/z* 23 $[Na]^+$ than *m/z* 40 $[Ca]^+$ due to the higher concentration of Na^+ vs. Ca^{2+} in seawater and also due to the lower ionization potential of Na vs. Ca (5.14 eV vs. 6.11 eV) (Gross et al., 2000). However, the ratio of *m/z* 23 $[Na]^+$ to *m/z* 40 $[Ca]^+$ in the OC-Ca particles is reversed, verifying a distinct single particle type (Gross et al., 2000; Gaston et al., 2011). Similarly, the ion signal of *m/z* 39 $[K]^+$ does not surpass that of *m/z* 40 $[Ca]^+$ in OC-Ca, although K is ionized more easily than Ca (4.34 eV vs. 6.11eV) (Gross et al., 2000). Although RH at the sampling outlet was < 40%, the short residence time of the particles within the drying tube (< 5 s) and vacuum system (< 1 ms) could have been insufficient for the complete efflorescence of SSAs (Gaston et al., 2011; Sierau et al., 2014). Hence, the OC-Ca could not be attributed to the chemical fractionation of the efflorescence SSAs in SPAMS analysis. Additionally, based on the single-particle mass spectrometry technique, some particle types with similar chemical characteristics to OC-Ca have been observed in both field and laboratory studies (e.g., atomization of sea ice meltwater collected in the Southern Ocean) (Gaston et al., 2011; Prather et al., 2013; Collins et al., 2014; Guasco et al., 2014; Dall'osto et al., 2019; Su et al., 2021). The OC-Ca may be from local emissions because the measurements were almost entirely influenced by polar air masses (**Fig. S1**). Other possible sources, such as glacial dust (Tobo et al., 2019), could be excluded because of the lack of crustal mass spectral characteristics (e.g., -76 $[SiO_3]^-$, 27 $[Al]^+$, and 48 $[Ti]^+$/64 $[TiO]^+$) (Pratt et al., 2009; Zawadowicz et al., 2017). And the mean mass concentration ratio of Ca/Na in the aerosol sample was only 0.10, much lower than that in the crust (1.78, w/w).

In contrast, SS-Ca was classified as a pure inorganic cluster with predominant contributions of Na-related compounds (*m/z* 23 $[Na]^+$, 46 $[Na_2]^+$, 81/83 $[Na_2{}^{35/37}Cl]^+$, and -93/-95 $[Na^{35/37}Cl_2]^-$), Mg (*m/z* 24), K (*m/z* 39), and Ca (*m/z* 40) in the mass spectra (**Fig. 6a**). Organic ion signals such as organic nitrogen (*m/z* -26 $[CN]^-$ and -42 $[CNO]^-$) and phosphate (*m/z* -63 $[PO_2]^-$ and -79 $[PO_3]^-$) were rarely detected (~1%, by NF). As described above, these compounds relate to oceanic biogeochemical processes. In addition, secondary species (e.g., nitrate of *m/z* -62 $[NO_3]^-$ and sulfate of *m/z* -97 $[HSO_4]^-$) were also not observed, indicating a fresh origin and/or less atmospheric aging. As a subpopulation of SS, SS-Ca may originate from bubble bursting within open water and/or blowing snow.

4 Discussion

SS-Ca (calcium-containing sea salt) represents a mixture of NaCl and $CaCl_2$. However, the SS-Ca showed a weak correlation ($r = 0.21$, $p < 0.05$, by count and $r = 0.03$, $p < 0.05$, by the peak area of *m/z* 40 $[Ca]^+$) with the mass concentration of Ca^{2+} **(Table 1)**. In addition, the proportion of SS-Ca was also small (11.6%, **Fig. 6h**). These results indicate that $CaCl_2$ is not the major reason for the Ca^{2+} enrichment in SSAs, although $CaCl_2$ has been proposed as a cause, based on laboratory atomizing of pure inorganic artificial seawater (Salter et al., 2016). The contribution of ikaite ($CaCO_3 \cdot 6H_2O$) could also be excluded due to its low water solubility (Bischoff et al., 1993; Dieckmann et al., 2008; Dieckmann et al., 2010), although ikaite from sea salt fractionation has also been proposed to account for the Ca^{2+} enrichment in SSAs over the Antarctic coast (Hara et al., 2012). Moreover, the mass spectral signatures of $CaCO_3$ (e.g., *m/z* 56 $[CaO]^+$ and -60 $[CO_3]^{2-}$ (see Sullivan et al. (2009)) were also rare in the SS-Ca particles (**Fig. 6a**).

As a major component (~ 72%, by occurrence frequency) of the Ca-containing particles, OC-Ca is expected to be partially responsible for the calcium enrichment in SSAs. First, the OC-Ca and mass concentration of Ca^{2+} exhibited moderately weak positive correlations (r = 0.42, $p < 0.05$, by count and r = 0.49, $p < 0.05$, by the peak area of *m/z* 40 $[Ca]^+$) and moderately strong correlations under higher EF_{Ca} values ($EF_{Ca} > 10$, r = 0.63, $p < 0.05$, by count and r = 0.68, $p < 0.05$, by the peak area of *m/z* 40 $[Ca]^+$) (Table 1). Also, such correlations were great during leg I (r = 0.59, $p < 0.05$, by count and r = 0.60, $p < 0.05$, by the peak area of *m/z* 40 $[Ca]^+$). Second, the OC-Ca showed a size distribution with a peak at 1 μm (**Fig. 6i**), which is consistent with the significant Ca^{2+} enrichment that is generally found in submicron SSAs (Cochran et al., 2016; Salter et al., 2016; Mukherjee et al., 2020).

We further show that calcium may strongly mix with organic matter, probably as organically complexed calcium, in the OC-Ca particles. The calcium correlated well with different kinds of organic matter (e.g., phosphate, r = 0.81, $p < 0.05$, by the peak area), but poorly correlated with chloride (r = 0.21, $p < 0.05$, by the peak area and r = 0.48, $p < 0.05$, by mass concentration) (**Fig. S6**). In addition, different kinds of organic matter (e.g., organic nitrogen, organic carbon, etc.) in the OC-Ca particles also showed enrichment trends below the submicron level, analogously to Ca^{2+} enrichment (**Fig. S8**). Particularly, EF_{Ca} and organic nitrogen (with the largest NF in OC-Ca) were both affected by the environmental factors of ambient temperature, wind speed, and sea ice fraction, indicating possible organic binding with calcium (**Fig. S9**).

To exclude the potential inorganic water-soluble compounds (i.e., chloride (*m/z* -35 and -37), nitrate (*m/z* -62), and sulfate (*m/z* -97)), we further classified OC-Ca into two subpopulations, OC-Ca-Organic (23.6%, by proportion) and OC-Ca-Inorganic (48.7%, by proportion) (**Fig. S10**),

depending on the presence of inorganic ion signals (i.e., chloride of *m/z* -35/-37 $[Cl]^-$, nitrate of *m/z* -62 $[NO_3]^-$, and sulfate of *m/z* -97 $[HSO_4]^-$). Both the OC-Ca types and mass concentrations of Ca^{2+} showed enhanced correlations under high EF_{Ca} values (**Table 1**). In particular, OC-Ca-Organic exhibited stronger correlations than did OC-Ca-Inorganic ($r = 0.51$ vs. $r = 0.28$, $p < 0.05$, by count and $r = 0.51$ vs. 0.31, $p < 0.05$, by the peak area of *m/z* 40 $[Ca]^+$, respectively), which indicates the importance of OC-Ca-Organic for the enrichment of Ca^{2+}. Although we did not measure the hygroscopicity of the OC-Ca in this study, we infer it to be hygroscopic to some extent. As reported by Cochran et al. (2017), the mixture of sea salt with organic matter can also exhibit a certain hygroscopicity (hygroscopicity parameter, 0.50-1.27). Therefore, it is likely that the organically complexed calcium is slightly water-soluble and is partially responsible for calcium enrichment, while current studies may neglect it.

The possible processes contributing to the calcium enrichment induced by OC-Ca can only be speculated on (**Fig. 7**). Ca^{2+} tends to bind with organic matter of biogenic origin, such as exopolymer substances (EPSs), and subsequently assemble as marine microgels (Verdugo et al., 2004; Gaston et al., 2011; Krembs et al., 2011; Orellana et al., 2011; Verdugo, 2012; Orellana et al., 2021). Large amounts of microgels, driven by sea ice algae, microorganisms, and/or exchanges of organic matter with the seawater below, stick to the sea ice due to its porous nature. And they are likely to present in the snow, frost flowers, and brine channels (Krembs et al., 2002; Gao et al., 2012; Vancoppenolle et al., 2013; Arrigo, 2014; Boetius et al., 2015; Kirpes et al., 2019). A low wind speed may not only be conducive to the formation of frost flowers and snow but also produce less sea salt (i.e., small yields of Na^+ relative to Ca^{2+}) (Rankin et al., 2002). Correspondingly, a high wind speed (≥ 7 m s^{-1}) can yield more sea salt by blowing-snow events

and/or wave breaking (Yang et al., 2008; Song et al., 2022), presenting a dilution effect of Na^+ on Ca^{2+}. In this case, the calcium enrichment in SSAs could reasonably be attributed to the possible gel-like calcium-containing particles released by low-wind-blown sea ice. This inference is supported by the observation of air masses blown over a large fraction of sea ice/ land-based Antarctic ice, as well as a moderate negative correlation ($r = 0.50$, $p < 0.001$) between wind speed and sea ice fraction. In addition, we also observed a higher proportion of OC-Ca at low wind speeds (< 7 m s^{-1}, 61.5%) than at high wind speeds (≥ 7 m s^{-1}, 38.5%). Coincidently, Song et al. (2022) also reported that a low wind-blown sea ice process can drive the biogenic aerosol response in the high Arctic. In addition, the enhanced presence of film drops was observed at lower wind speeds (< 6 m s^{-1}) (Norris et al., 2011), which suggests that the bubble bursts within the sea ice leads and open water may also be responsible for the release of OC-Ca and its calcium enrichment involved (Leck and Bigg, 2005b, a; Bigg and Leck, 2008; Leck and Bigg, 2010; Leck et al., 2013; Kirpes et al., 2019).

As expected, the results of the Ca^{2+} enrichment in SSAs obtained from ion mass concentration via IGAC did not fully align with results from SPAMS datasets. We propose two possible explanations for this discrepancy: (i) It could be attributed to a difference in the size of particles collected by the two different instruments (~ 10 μm for IGAC and 0.2–2 μm for SPAMS). In addition, SPAMS cannot measure the Aitken-mode particles (Sierau et al., 2014), and can measure only the tail of accumulation-mode particles with a relatively low hit rate (~11% in this study). (ii) The types of datasets obtained via IGAC (ion mass concentration) and SPAMS (mass spectral characteristics) are different. The former method partially reflects the Ca^{2+} distribution based on water-soluble Ca^{2+}, while the OC-Ca measured by SPAMS may have low water

417 solubility. The latter method is still challenging to use for quantitative measurements due to
418 potential inhomogeneities in the transmission efficiencies of the aerodynamic lenses and
419 desorption/ionization, as well as the matrix effects of individual particles (Gross et al., 2000; Qin
420 et al., 2006; Pratt and Prather, 2012). Therefore, it may not be straightforward to compare the
421 particle count and peak area with the absolute mass concentration.

422 Although there is a discrepancy between the two instruments, we believe our results to be
423 reliable and representative. On the one side, the quantitative results concluded by IGAC confirm
424 the enrichment of Ca^{2+} in SSAs and demonstrate their dependence on and relevance to the
425 environmental factors. On the other side, the individual particle analysis ranging in size from 0.2
426 to 2 μm is highly appropriate for revealing the calcium distribution in SSAs, as previous studies
427 have shown increasing Ca^{2+} enrichment in SSAs below 1 μm (Oppo et al., 1999; Hara et al., 2012;
428 Cochran et al., 2016; Salter et al., 2016; Mukherjee et al., 2020). Our study successfully identifies
429 a unique calcareous particle type (i.e., OC-Ca) and its specific mixing state. A comprehensive
430 understanding of the characteristics of OC-Ca to the mechanisms of calcium enrichment is
431 essential for further recognizing the CCN and IN activation in remote marine areas.

432 Another limitation is that only several environmental factors were considered for calcium
433 enrichment in this study. Some potential factors, such as surface net solar radiation, snowfall, total
434 cloud cover, surface pressure, total precipitation, boundary layer height, seawater salinity, etc.,
435 may also affect the calcium enrichment in SSAs through regulating the yield of sea salt (i.e., Na^{+}
436 mass concentration) (Song et al., 2022). However, they were not available in this study because of
437 the lack of measurement during the cruise. Meanwhile, the satellite data with low temporal-spatial
438 resolution cannot match per hour in each starting condition. We hope that future research will

439 further investigate the enrichment of specific species in SSAs under a wider range of
440 meteorological or oceanographic conditions.

441 **5 Conclusions and atmospheric implications**

442 We investigated the distribution of calcium in SSAs through the R/V *Xuelong* cruise
443 observation campaigns over the Ross Sea, Antarctica. The most significant Ca^{2+} enrichment in
444 SSAs occurred under relatively lower ambient temperatures (< -3.5 ℃) and wind speeds (< 7 m s^{-1})
445 and with the presence of sea ice. With the help of individual particle mass spectral analysis, we
446 first propose that a single-particle type of OC-Ca (internally mixed organics with calcium),
447 probably resulting from the preferential binding of Ca^{2+} with organic matter, could partially
448 account for the calcium enrichment in SSAs. We speculate that OC-Ca is likely produced from the
449 effects of low wind-blown sea ice on microgels induced by Ca^{2+} and/or the bubble bursts in the
450 open-water and/or sea ice leads. However, the impact of environmental factors and OC-Ca on
451 calcium enrichment in SSAs still cannot be well predicted by multiple linear regression and
452 random forest analysis (**SI text S5**), which may be ascribed to other unknown mechanisms and/or
453 organically complexed calcium with low water solubility. In addition, our conclusions based on
454 limited spatial, temporal, meteorological, and oceanographic conditions may not be accessible to
455 other seasons and oceanic basins.

456 We suggest that the environmental behaviors of the possible gel-like calcium-containing
457 particles (i.e., OC-Ca) should be paid more attention behind the mechanisms of calcium
458 enrichment. Under the stimulation of specific environmental factors (e.g., pH, temperature,
459 chemical compounds, pollutants, and UV radiation), their physicochemical properties would be

changed (e.g., water-solubility enhanced by the cleavage of polymers) (Orellana and Verdugo, 2003; Orellana et al., 2011). Such particles may be preferred candidates for CCN and/or IN (Willis et al., 2018; Lawler et al., 2021). To our knowledge, this is the first report of a calcium-dominated single-particle type OC-Ca in the Antarctic. In the context of global warming and sea ice retreat, this work provides insight into the chemical composition and distribution of submicron SSAs in the Antarctic summer atmosphere, which would be helpful for a better understanding of aerosol-cloud-climate interactions.

Data Availability Statement

The data are available at Zenodo (https://doi.org/10.5281/zenodo.7276073). Details can be accessed by contacting the corresponding author Guohua Zhang (zhanggh@gig.ac.cn) and the first author Bojiang Su (subojiang21@mails.ucas.ac.cn).

Declaration of Competing Interest

The authors declare that they have no known competing financial interests or personal relationships that could have appeared to influence the work reported in this paper.

Author Contributions

The idea for the study was conceived by BJS. BJS analyzed the data, prepared the figures, and wrote the manuscript under the guidance of GHZ and XYB. LL and JPY contributed to the observation data. All co-authors contributed to the discussions of the results and refinement of the manuscript.

Acknowledgment

This work was supported by the Guangdong Basic and Applied Basic Research Foundation (2019B151502022), the National Natural Science Foundation of China (42077322 and 42130611), the Youth Innovation Promotion Association CAS (2021354), and the Guangdong Foundation for Program of Science and Technology Research (2020B1212060053). The authors would like to thank the editor and reviewers for their valuable time and feedback.

485 **Figure captions**

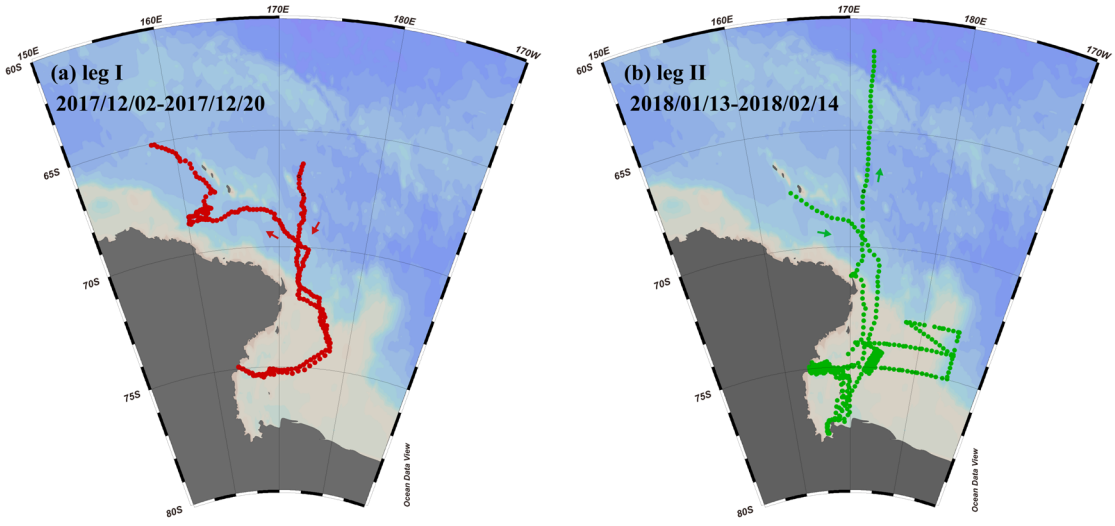

486

487 **Figure 1**

488 Observation campaigns through R/V *Xuelong* in the Ross Sea, Antarctic. (a) Leg I took place from

489 December 2-20, 2017. (b) Leg II was conducted from January 13 to February 14, 2018.

490

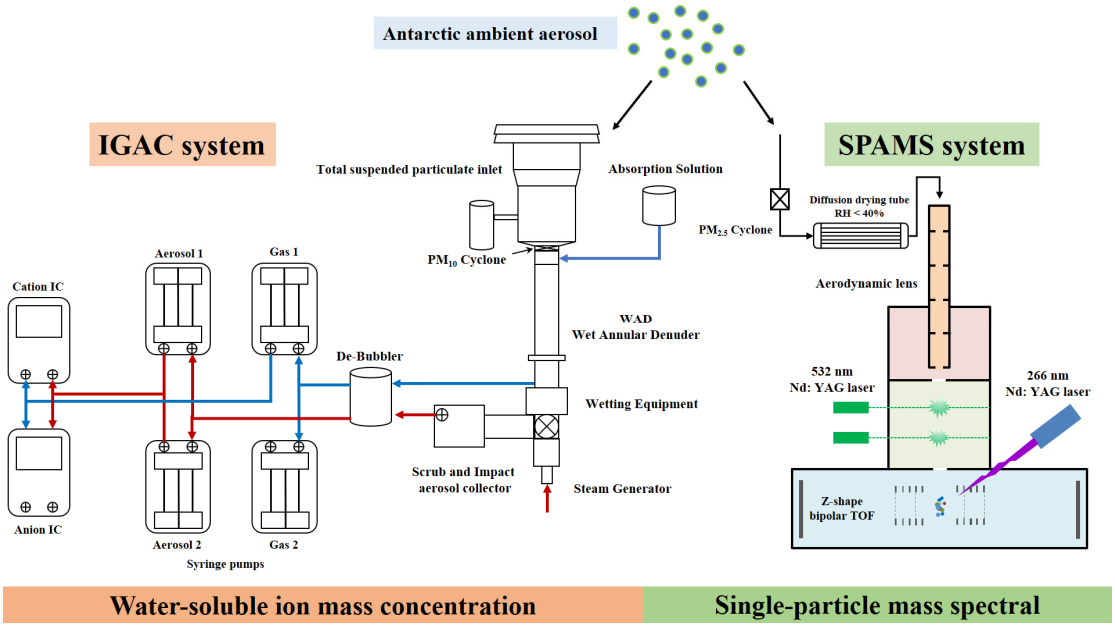

491

492 **Figure 2**

493 A schematic of the aerosol sampling system of IGAC and SPAMS during the research cruise over

494 the Ross Sea, Antarctic.

495

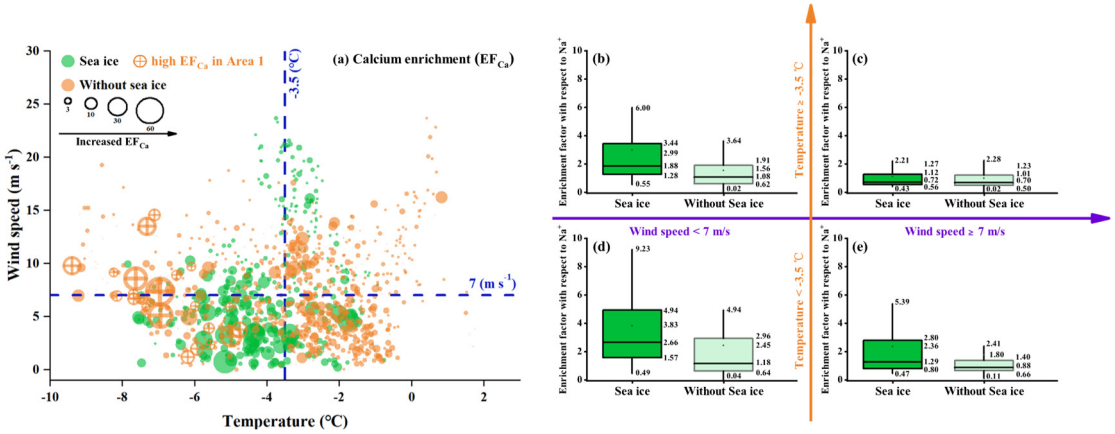

496

497 **Figure 3**

498 (a) Bubble chart of the hourly Ca^{2+} enrichment factor (EF_{Ca}) with respect to Na^+ with different
499 environmental factors (ambient temperature, wind speed, and sea ice fraction). The green and
500 orange dots represent the EF_{Ca} values for the periods with and without sea ice, respectively. The
501 orange marked dots represent a series of high EF_{Ca} cases that were correlated with a high
502 concentration of chlorophyll-a during leg II of the cruise. (b)-(e) Data support of the bubble chart
503 represented by box and whisker plots. In the box and whisker plots, the marked values from top to
504 bottom are the 90th and 75th percentiles, mean, median, and 25th and 10th percentiles,
505 respectively.

506

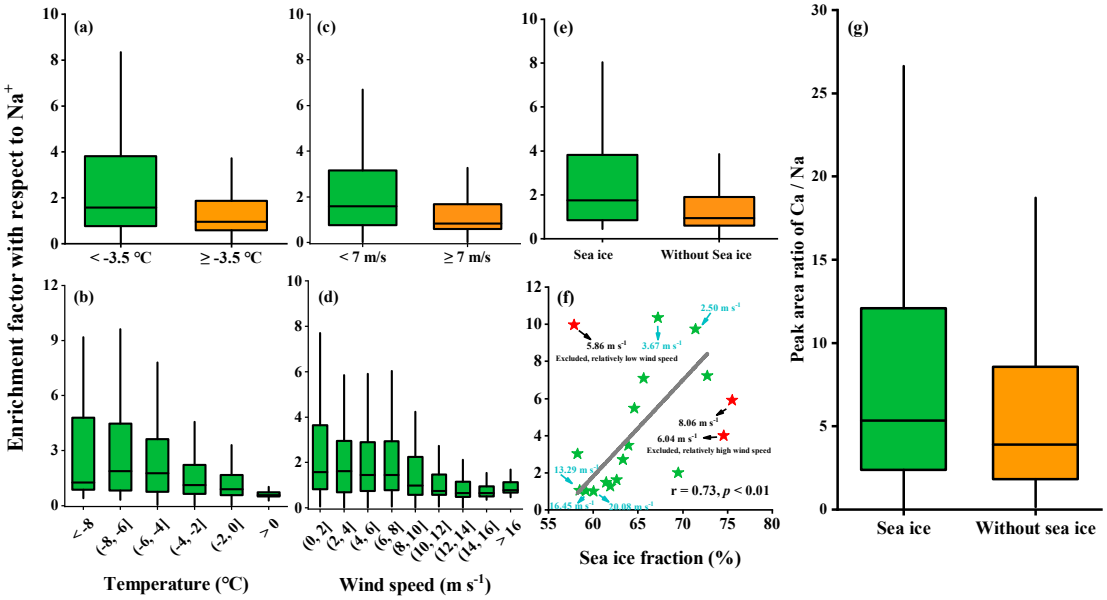

507

508 **Figure 4**

509 Enrichment factors of Ca^{2+} with respect to Na^{+} varied as a function of the ambient temperature (a-
510 b), wind speed (c-d), and sea ice fraction (e-f) during cruise observation campaigns. (g) A box and
511 whisker plot of the single-particle peak area ratio of Ca/Na in OC-Ca for the periods with and
512 without sea ice. In the box and whisker plots, the lower, median, and upper lines of the box denote
513 the 25th, 50th, and 75th percentiles, respectively. The lower and upper edges denote the 10th and
514 90th percentiles, respectively. The black solid star (f) exhibited an anomalous trend due to its
515 nature of relatively high or low wind speed. The first point exhibited a high EF value because of
516 its relatively low wind speed (5.86 m s^{-1}). The second and third points exhibited low EF values
517 because of their relatively high wind speeds of 6.04 m s^{-1} and 8.06 m s^{-1}, respectively. These three
518 points have been excluded from the correlation analysis.

519

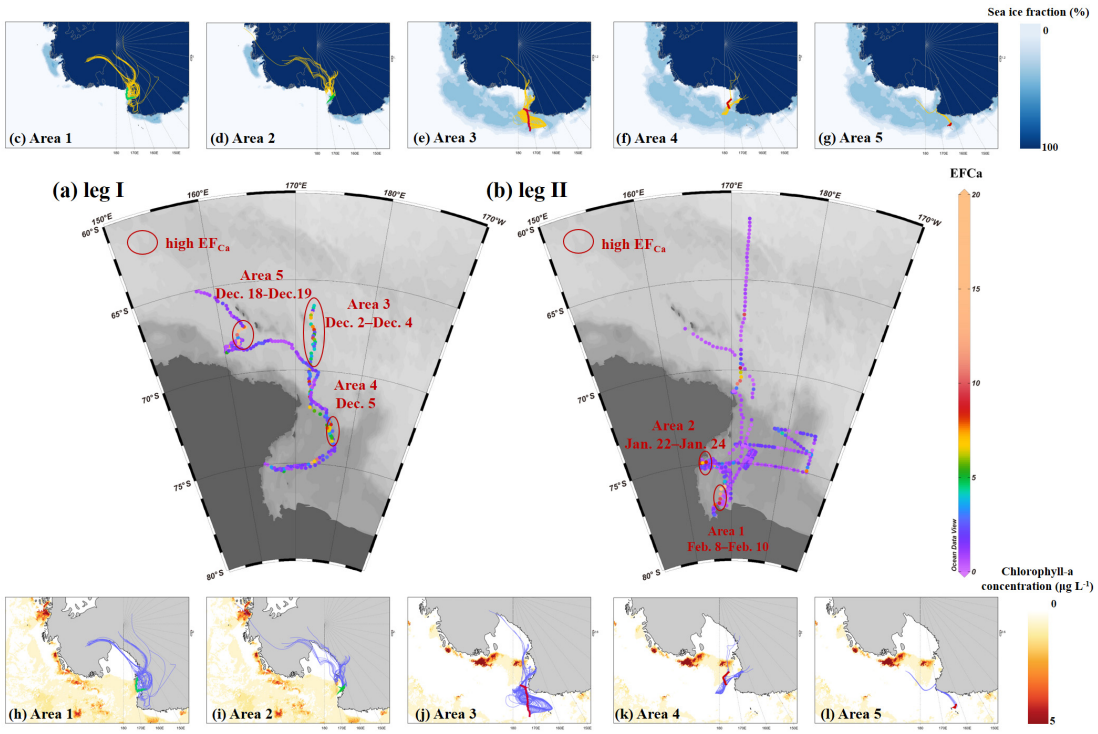

520

521 **Figure 5**

522 Distribution of EF_{Ca} during (a) leg I and (b) leg II. Five distinct areas with continuous enhanced

523 Ca^{2+} enrichment events, along with 96-hour back trajectories (one trajectory per hour in each

524 starting condition), sea ice fraction (c-g, yellow traces), and chlorophyll-a concentration (h-l, light-

525 blue traces). Lines in red and green referred to ship tracks for corresponding areas during leg I and

526 leg II, respectively.

527

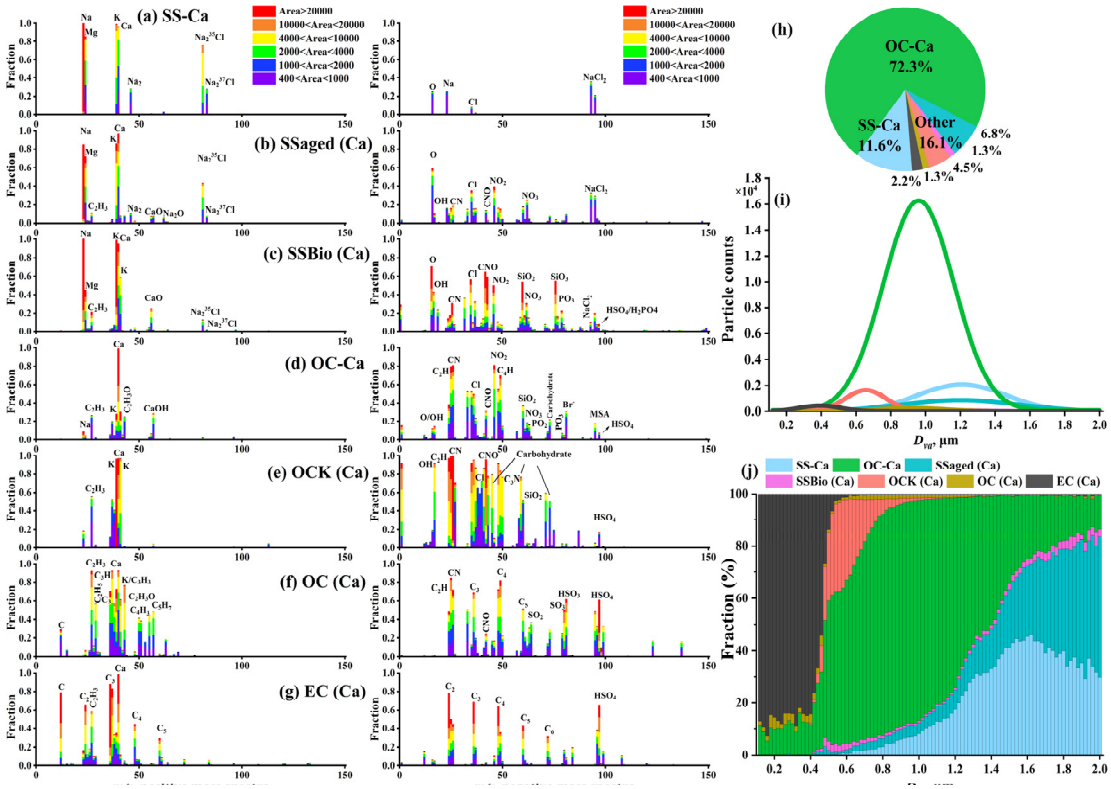

Figure 6

(a) – (g) Average digitized single-particle mass spectra of seven chemical classes of Ca-containing particles. New single-particle types are reclassified with *m/z* 40 [Ca^{2+}] based on previous ART-2a results. (h) Relative proportion and (i) unscaled size-resolved number distributions of single-particle types using Gaussian Fitting. (j) Number fractions of single-particle types per size bin versus particle size.

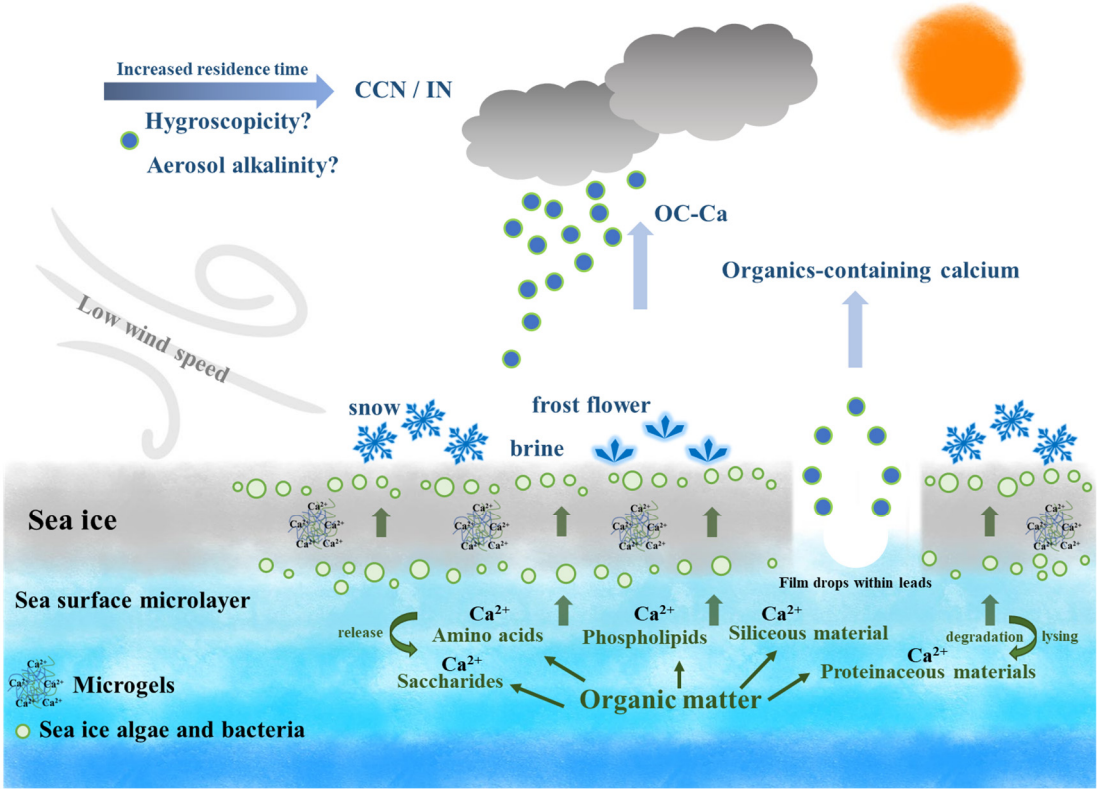

536

537 **Figure 7**

538 Schematic of the production of OC-Ca and its possible atmospheric implications beyond calcium
539 enrichment. Ca^{2+} tends to bind with organic matter whining sea ice/seawater, and subsequently
540 assemble to marine microgels, likely present in the snow, frost flowers, and brine channels. With
541 the low wind-blown sea ice process and/or bubble bursting within sea ice leads, these gel-like
542 particles (i.e., OC-Ca) may be released to the Antarctic atmosphere, as a potential source of
543 CCN/IN. Notably, the dataset via SPAMS cannot directly identify marine microgels. OC-Ca was
544 likely associated with marine microgels, as calcium and biological organic material were
545 extensively internally mixed. This OC-Ca type has previously been observed in the laboratory
546 simulation of Collins et al. (2014).

547

Table captions

EF_{Ca}	Count (Correlation coefficient, r)				Peak area (Correlation coefficient, r, *m/z* 40 $[Ca]^{2+}$)			
	OC-Ca-Inorganic	OC-Ca-Organic	OC-Ca	SS-Ca	OC-Ca-Inorganic	OC-Ca-Organic	OC-Ca	SS-Ca
0 - 5	0.08	0.31	0.18	0.07	0.18	0.44	0.41	0.04
5 - 10	0.15	0.37	0.27	0.04	0.14	0.36	0.33	0.06
> 10	0.58	0.59	0.63	0.10[a]	0.53	0.68	0.68	0.10
Leg I	0.45	0.59	0.55	0.02	0.53	0.60	0.60	0.03
Leg II	0.06	0.22	0.14	0.45	0.14	0.39	0.39	0.11
Total	0.28	0.51	0.42	0.21	0.31	0.51	0.49	0.03

a: *p* -value > 0.05
(Pearson method, two-tailed test)

Table 1

Correlation analysis between the OC-Ca (by count and by the peak area of *m/z* 40 $[Ca]^{+}$) and its two subpopulations OC-Ca-Organic and OC-Ca-Inorganic, SS-Ca (by count and by the peak area of *m/z* 40 $[Ca]^{+}$), and mass concentration of Ca^{2+} in the variation of EF_{Ca}, with the *p*-value < 0.05.

References

Arrigo, K. R.: Sea ice ecosystems, Ann Rev Mar Sci, 6, 439-467, https://doi.org/10.1146/annurev-marine-010213-135103, 2014.

Bertram, T. H., Cochran, R. E., Grassian, V. H., and Stone, E. A.: Sea spray aerosol chemical composition: elemental and molecular mimics for laboratory studies of heterogeneous and multiphase reactions, Chemical Society Reviews, 47, 2374-2400, https://doi.org/10.1039/c7cs00008a, 2018.

Bigg, E. K. and Leck, C.: The composition of fragments of bubbles bursting at the ocean surface, Journal of Geophysical Research: Atmospheres, 113https://doi.org/10.1029/2007jd009078, 2008.

Bischoff, J. L., Fitzpatrick, J. A., and Rosenbauer, R. J.: The Solubility and Stabilization of Ikaite (Caco3.6h2o) from 0-Degrees-C To 25-Degrees-C - Environmental and Paleoclimatic Implications for Thinolite Tufa, J Geol, 101, 21-33, https://doi.org/10.1086/648194, 1993.

Boetius, A., Anesio, A. M., Deming, J. W., Mikucki, J. A., and Rapp, J. Z.: Microbial ecology of the cryosphere: sea ice and glacial habitats, Nat Rev Microbiol, 13, 677-690, https://doi.org/10.1038/nrmicro3522, 2015.

Boreddy, S. K. R. and Kawamura, K.: A 12-year observation of water-soluble ions in TSP aerosols collected at a remote marine location in the western North Pacific: an outflow region of Asian dust, Atmos Chem Phys, 15, 6437-6453, https://doi.org/10.5194/acp-15-6437-2015, 2015.

Brooks, S. D. and Thornton, D. C. O.: Marine Aerosols and Clouds, Annu Rev Mar Sci, 10, 289-313, https://doi.org/10.1146/annurev-marine-121916-063148, 2018.

575 Carter-Fenk, K. A., Dommer, A. C., Fiamingo, M. E., Kim, J., Amaro, R. E., and Allen, H. C.: Calcium
576 bridging drives polysaccharide co-adsorption to a proxy sea surface microlayer, Phys Chem Chem
577 Phys, 23, 16401-16416, https://doi.org/10.1039/d1cp01407b, 2021.
578 Chi, J. W., Li, W. J., Zhang, D. Z., Zhang, J. C., Lin, Y. T., Shen, X. J., Sun, J. Y., Chen, J. M., Zhang, X.
579 Y., Zhang, Y. M., and Wang, W. X.: Sea salt aerosols as a reactive surface for inorganic and organic
580 acidic gases in the Arctic troposphere, Atmos Chem Phys, 15, 11341-11353,
581 https://doi.org/10.5194/acp-15-11341-2015, 2015.
582 Cochran, R. E., Jayarathne, T., Stone, E. A., and Grassian, V. H.: Selectivity Across the Interface: A
583 Test of Surface Activity in the Composition of Organic-Enriched Aerosols from Bubble Bursting, J
584 Phys Chem Lett, 7, 1692-1696, https://doi.org/10.1021/acs.jpclett.6b00489, 2016.
585 Cochran, R. E., Laskina, O., Trueblood, J. V., Estillore, A. D., Morris, H. S., Jayarathne, T., Sultana, C.
586 M., Lee, C., Lin, P., Laskin, J., Laskin, A., Dowling, J. A., Qin, Z., Cappa, C. D., Bertram, T. H.,
587 Tivanski, A. V., Stone, E. A., Prather, K. A., and Grassian, V. H.: Molecular Diversity of Sea Spray
588 Aerosol Particles: Impact of Ocean Biology on Particle Composition and Hygroscopicity, Chem., 2,
589 655-667, https://doi.org/10.1016/j.chempr.2017.03.007, 2017.
590 Collins, D. B., Zhao, D. F., Ruppel, M. J., Laskina, O., Grandquist, J. R., Modini, R. L., Stokes, M. D.,
591 Russell, L. M., Bertram, T. H., Grassian, V. H., Deane, G. B., and Prather, K. A.: Direct aerosol
592 chemical composition measurements to evaluate the physicochemical differences between
593 controlled sea spray aerosol generation schemes, Atmos Meas Tech, 7, 3667-3683,
594 https://doi.org/10.5194/amt-7-3667-2014, 2014.
595 Cravigan, L. T., Mallet, M. D., Vaattovaara, P., Harvey, M. J., Law, C. S., Modini, R. L., Russell, L. M.,
596 Stelcer, E., Cohen, D. D., Olsen, G., Safi, K., Burrell, T. J., and Ristovski, Z.: Sea spray aerosol
597 organic enrichment, water uptake and surface tension effects, Atmos Chem Phys, 20, 7955-7977,
598 https://doi.org/10.5194/acp-20-7955-2020, 2020.
599 Czerwieniec, G. A., Russell, S. C., Tobias, H. J., Pitesky, M. E., Fergenson, D. P., Steele, P., Srivastava,
600 A., Horn, J. M., Frank, M., Gard, E. E., and Lebrilla, C. B.: Stable isotope labeling of entire
601 Bacillus atrophaeus spores and vegetative cells using bioaerosol mass spectrometry, Anal Chem,
602 77, 1081-1087, https://doi.org/10.1021/ac0488098, 2005.
603 Dall'Osto, M., Airs, R. L., Beale, R., Cree, C., Fitzsimons, M. F., Beddows, D., Harrison, R. M.,
604 Ceburnis, D., O'Dowd, C., Rinaldi, M., Paglione, M., Nenes, A., Decesari, S., and Simo, R.:
605 Simultaneous Detection of Alkylamines in the Surface Ocean and Atmosphere of the Antarctic
606 Sympagic Environment, Acs Earth Space Chem, 3, 854-862,
607 https://doi.org/10.1021/acsearthspacechem.9b00028, 2019.
608 Dieckmann, G., Nehrke, G., Uhlig, C., Göttlicher, J., Gerland, S., Granskog, M., and Thomas, D.: Brief
609 Communication: Ikaite (CaCO3·6H2O) discovered in Arctic sea ice, The Cryosphere, 4, 227-230,
610 https://doi.org/10.5194/tc-4-227-2010, 2010.
611 Dieckmann, G., Nehrke, G., Papadimitriou, S., Göttlicher, J., Steininger, R., Kennedy, H., Wolf-
612 Gladrow, D., and Thomas, D.: Calcium carbonate as ikaite crystals in Antarctic sea ice, Geophys
613 Res Lett, 35https://doi.org/10.1029/2008gl033540, 2008.
614 Facchini, M. C., Rinaldi, M., Decesari, S., Carbone, C., Finessi, E., Mircea, M., Fuzzi, S., Ceburnis, D.,
615 Flanagan, R., Nilsson, E. D., de Leeuw, G., Martino, M., Woeltjen, J., and O'Dowd, C. D.: Primary
616 submicron marine aerosol dominated by insoluble organic colloids and aggregates, Geophys Res
617 Lett, 35https://doi.org/10.1029/2008gl034210, 2008.
618 Gao, Q., Leck, C., Rauschenberg, C., and Matrai, P. A.: On the chemical dynamics of extracellular

polysaccharides in the high Arctic surface microlayer, Ocean Sci, 8, 401-418, https://doi.org/10.5194/os-8-401-2012, 2012.

Gaston, C. J., Furutani, H., Guazzotti, S. A., Coffee, K. R., Bates, T. S., Quinn, P. K., Aluwihare, L. I., Mitchell, B. G., and Prather, K. A.: Unique ocean-derived particles serve as a proxy for changes in ocean chemistry, Journal of Geophysical Research: Atmospheres, 116https://doi.org/10.1029/2010jd015289, 2011.

Gross, D. S., Galli, M. E., Silva, P. J., and Prather, K. A.: Relative sensitivity factors for alkali metal and ammonium cations in single particle aerosol time-of-flight mass spectra, Anal Chem, 72, 416-422, https://doi.org/10.1021/ac990434g, 2000.

Guasco, T. L., Cuadra-Rodriguez, L. A., Pedler, B. E., Ault, A. P., Collins, D. B., Zhao, D. F., Kim, M. J., Ruppel, M. J., Wilson, S. C., Pomeroy, R. S., Grassian, V. H., Azam, F., Bertram, T. H., and Prather, K. A.: Transition Metal Associations with Primary Biological Particles in Sea Spray Aerosol Generated in a Wave Channel, Environ Sci Technol, 48, 1324-1333, https://doi.org/10.1021/es403203d, 2014.

Hara, K., Osada, K., Yabuki, M., and Yamanouchi, T.: Seasonal variation of fractionated sea-salt particles on the Antarctic coast, Geophys Res Lett, 39https://doi.org/10.1029/2012gl052761, 2012.

Keene, W. C., Maring, H., Maben, J. R., Kieber, D. J., Pszenny, A. A. P., Dahl, E. E., Izaguirre, M. A., Davis, A. J., Long, M. S., Zhou, X. L., Smoydzin, L., and Sander, R.: Chemical and physical characteristics of nascent aerosols produced by bursting bubbles at a model air-sea interface, Journal of Geophysical Research: Atmospheres, 112https://doi.org/10.1029/2007jd008464, 2007.

Kirpes, R. M., Bonanno, D., May, N. W., Fraund, M., Barget, A. J., Moffet, R. C., Ault, A. P., and Pratt, K. A.: Wintertime Arctic Sea Spray Aerosol Composition Controlled by Sea Ice Lead Microbiology, Acs Central Sci, 5, 1760-1767, https://doi.org/10.1021/acscentsci.9b00541, 2019.

Köllner, F., Schneider, J., Willis, M. D., Klimach, T., Helleis, F., Bozem, H., Kunkel, D., Hoor, P., Burkart, J., Leaitch, W. R., Aliabadi, A. A., Abbatt, J. P. D., Herber, A. B., and Borrmann, S.: Particulate trimethylamine in the summertime Canadian high Arctic lower troposphere, Atmos Chem Phys, 17, 13747-13766, https://doi.org/10.5194/acp-17-13747-2017, 2017.

Krembs, C., Eicken, H., and Deming, J. W.: Exopolymer alteration of physical properties of sea ice and implications for ice habitability and biogeochemistry in a warmer Arctic, P Natl Acad Sci USA, 108, 3653-3658, https://doi.org/10.1073/pnas.1100701108, 2011.

Krembs, C., Eicken, H., Junge, K., and Deming, J. W.: High concentrations of exopolymeric substances in Arctic winter sea ice: implications for the polar ocean carbon cycle and cryoprotection of diatoms, Deep-Sea Res Pt I, 49, 2163-2181, https://doi.org/10.1016/S0967-0637(02)00122-X, 2002.

Lawler, M. J., Saltzman, E. S., Karlsson, L., Zieger, P., Salter, M., Baccarini, A., Schmale, J., and Leck, C.: New Insights Into the Composition and Origins of Ultrafine Aerosol in the Summertime High Arctic, Geophys Res Lett, 48https://doi.org/10.1029/2021gl094395, 2021.

Leck, C. and Bigg, E. K.: Source and evolution of the marine aerosol - A new perspective, Geophys Res Lett, 32https://doi.org/10.1029/2005gl023651, 2005a.

Leck, C. and Bigg, E. K.: Biogenic particles in the surface microlayer and overlaying atmosphere in the central Arctic Ocean during summer, Tellus B, 57, 305-316, https://doi.org/10.1111/j.1600-0889.2005.00148.x, 2005b.

Leck, C. and Bigg, E. K.: New Particle Formation of Marine Biological Origin, Aerosol Sci Tech, 44, 570-577, https://doi.org/10.1080/02786826.2010.481222, 2010.

Leck, C. and Svensson, E.: Importance of aerosol composition and mixing state for cloud droplet activation over the Arctic pack ice in summer, Atmos Chem Phys, 15, 2545-2568, https://doi.org/10.5194/acp-15-2545-2015, 2015.

Leck, C., Gao, Q., Mashayekhy Rad, F., and Nilsson, U.: Size-resolved atmospheric particulate polysaccharides in the high summer Arctic, Atmos Chem Phys, 13, 12573-12588, https://doi.org/10.5194/acp-13-12573-2013, 2013.

Li, L., Huang, Z., Dong, J., Li, M., Gao, W., Nian, H., Fu, Z., Zhang, G., Bi, X., Cheng, P., and Zhou, Z.: Real time bipolar time-of-flight mass spectrometer for analyzing single aerosol particles, Int J Mass Spectrom, 303, 118-124, https://doi.org/10.1016/j.ijms.2011.01.017, 2011.

Liu, Z. M., Lu, X. H., Feng, J. L., Fan, Q. Z., Zhang, Y., and Yang, X.: Influence of Ship Emissions on Urban Air Quality: A Comprehensive Study Using Highly Time-Resolved Online Measurements and Numerical Simulation in Shanghai, Environ Sci Technol, 51, 202-211, https://doi.org/10.1021/acs.est.6b03834, 2017.

Mukherjee, P., Reinfelder, J. R., and Gao, Y.: Enrichment of calcium in sea spray aerosol in the Arctic summer atmosphere, Mar Chem, 227https://doi.org/10.1016/j.marchem.2020.103898, 2020.

Murphy, D. M., Anderson, J. R., Quinn, P. K., McInnes, L. M., Brechtel, F. J., Kreidenweis, S. M., Middlebrook, A. M., Posfai, M., Thomson, D. S., and Buseck, P. R.: Influence of sea-salt on aerosol radiative properties in the Southern Ocean marine boundary layer, Nature, 392, 62-65, https://doi.org/10.1038/32138, 1998.

Norris, S. J., Brooks, I. M., de Leeuw, G., Sirevaag, A., Leck, C., Brooks, B. J., Birch, C. E., and Tjernstrom, M.: Measurements of bubble size spectra within leads in the Arctic summer pack ice, Ocean Sci, 7, 129-139, https://doi.org/10.5194/os-7-129-2011, 2011.

Oppo, C., Bellandi, S., Innocenti, N. D., Stortini, A. M., Loglio, G., Schiavuta, E., and Cini, R.: Surfactant components of marine organic matter as agents for biogeochemical fractionation and pollutant transport via marine aerosols, Mar Chem, 63, 235-253, https://doi.org/10.1016/S0304-4203(98)00065-6, 1999.

Orellana, M. V. and Verdugo, P.: Ultraviolet radiation blocks the organic carbon exchange between the dissolved phase and the gel phase in the ocean, Limnol Oceanogr, 48, 1618-1623, https://doi.org/10.4319/lo.2003.48.4.1618, 2003.

Orellana, M. V., Hansell, D. A., Matrai, P. A., and Leck, C.: Marine Polymer-Gels' Relevance in the Atmosphere as Aerosols and CCN, Gels, 7https://doi.org/10.3390/gels7040185, 2021.

Orellana, M. V., Matrai, P. A., Leck, C., Rauschenberg, C. D., Lee, A. M., and Coz, E.: Marine microgels as a source of cloud condensation nuclei in the high Arctic, P Natl Acad Sci USA, 108, 13612-13617, https://doi.org/10.1073/pnas.1102457108, 2011.

Passig, J., Schade, J., Irsig, R., Li, L., Li, X., Zhou, Z., Adam, T., and Zimmermann, R.: Detection of ship plumes from residual fuel operation in emission control areas using single-particle mass spectrometry, Atmos Meas Tech, 14, 4171-4185, https://doi.org/10.5194/amt-14-4171-2021, 2021.

Prather, K. A., Bertram, T. H., Grassian, V. H., Deane, G. B., Stokes, M. D., DeMott, P. J., Aluwihare, L. I., Palenik, B. P., Azam, F., Seinfeld, J. H., Moffet, R. C., Molina, M. J., Cappa, C. D., Geiger, F. M., Roberts, G. C., Russell, L. M., Ault, A. P., Baltrusaitis, J., Collins, D. B., Corrigan, C. E., Cuadra-Rodriguez, L. A., Ebben, C. J., Forestieri, S. D., Guasco, T. L., Hersey, S. P., Kim, M. J., Lambert, W. F., Modini, R. L., Mui, W., Pedler, B. E., Ruppel, M. J., Ryder, O. S., Schoepp, N. G., Sullivan, R. C., and Zhao, D. F.: Bringing the ocean into the laboratory to probe the chemical complexity of sea spray aerosol, P Natl Acad Sci USA, 110, 7550-7555,

https://doi.org/10.1073/pnas.1300262110, 2013.
Pratt, K. A. and Prather, K. A.: Mass spectrometry of atmospheric aerosolsuRecent developments and applications. Part II: On-line mass spectrometry techniques, Mass Spectrom Rev, 31, 17-48, https://doi.org/10.1002/mas.20330, 2012.
Pratt, K. A., DeMott, P. J., French, J. R., Wang, Z., Westphal, D. L., Heymsfield, A. J., Twohy, C. H., Prenni, A. J., and Prather, K. A.: In situ detection of biological particles in cloud ice-crystals, Nat Geosci, 2, 397-400, https://doi.org/10.1038/Ngeo521, 2009.
Qin, X. Y., Bhave, P. V., and Prather, K. A.: Comparison of two methods for obtaining quantitative mass concentrations from aerosol time-of-flight mass spectrometry measurements, Anal Chem, 78, 6169-6178, https://doi.org/10.1021/ac060395q, 2006.
Quinn, P. K., Collins, D. B., Grassian, V. H., Prather, K. A., and Bates, T. S.: Chemistry and Related Properties of Freshly Emitted Sea Spray Aerosol, Chem Rev, 115, 4383-4399, https://doi.org/10.1021/cr500713g, 2015.
Rankin, A. M., Wolff, E. W., and Martin, S.: Frost flowers: Implications for tropospheric chemistry and ice core interpretation, Journal of Geophysical Research: Atmospheres, 107, AAC 4-1-AAC 4-15, https://doi.org/10.1029/2002jd002492, 2002.
Russell, L. M., Hawkins, L. N., Frossard, A. A., Quinn, P. K., and Bates, T. S.: Carbohydrate-like composition of submicron atmospheric particles and their production from ocean bubble bursting, P Natl Acad Sci USA, 107, 6652-6657, https://doi.org/10.1073/pnas.0908905107, 2010.
Salter, M. E., Hamacher-Barth, E., Leck, C., Werner, J., Johnson, C. M., Riipinen, I., Nilsson, E. D., and Zieger, P.: Calcium enrichment in sea spray aerosol particles, Geophys Res Lett, 43, 8277-8285, https://doi.org/10.1002/2016gl070275, 2016.
Schill, S. R., Collins, D. B., Lee, C., Morris, H. S., Novak, G. A., Prather, K. A., Quinn, P. K., Sultana, C. M., Tivanski, A. V., Zimmermann, K., Cappa, C. D., and Bertram, T. H.: The Impact of Aerosol Particle Mixing State on the Hygroscopicity of Sea Spray Aerosol, Acs Central Sci, 1, 132-141, https://doi.org/10.1021/acscentsci.5b00174, 2015.
Sierau, B., Chang, R. Y. W., Leck, C., Paatero, J., and Lohmann, U.: Single-particle characterization of the high-Arctic summertime aerosol, Atmos Chem Phys, 14, 7409-7430, https://doi.org/10.5194/acp-14-7409-2014, 2014.
Sievering, H.: Aerosol non-sea-salt sulfate in the remote marine boundary layer under clear-sky and normal cloudiness conditions: Ocean-derived biogenic alkalinity enhances sea-salt sulfate production by ozone oxidation, Journal of Geophysical Research: Atmospheres, 109https://doi.org/10.1029/2003jd004315, 2004.
Song, C., Becagli, S., Beddows, D. C. S., Brean, J., Browse, J., Dai, Q., Dall'Osto, M., Ferracci, V., Harrison, R. M., Harris, N., Li, W., Jones, A. E., Kirchgäßner, A., Kramawijaya, A. G., Kurganskiy, A., Lupi, A., Mazzola, M., Severi, M., Traversi, R., and Shi, Z.: Understanding Sources and Drivers of Size-Resolved Aerosol in the High Arctic Islands of Svalbard Using a Receptor Model Coupled with Machine Learning, Environ Sci Technol, 56, 11189-11198, https://doi.org/10.1021/acs.est.1c07796, 2022.
Song, X. and Hopke, P. K.: Classification of single particles analyzed by ATOFMS using an artificial neural network, ART-2A, Anal Chem, 71, 860-865, https://doi.org/10.1021/ac9809682, 1999.
Srivastava, A., Pitesky, M. E., Steele, P. T., Tobias, H. J., Fergenson, D. P., Horn, J. M., Russell, S. C., Czerwieniec, G. A., Lebrilla, C. S., Gard, E. E., and Frank, M.: Comprehensive assignment of mass spectral signatures from individual Bacillus atrophaeus spores in matrix-free laser

751 desorption/ionization bioaerosol mass spectrometry, Anal Chem, 77, 3315-3323,
752 https://doi.org/10.1021/ac048298p, 2005.
753 Su, B., Wang, T., Zhang, G., Liang, Y., Lv, C., Hu, Y., Li, L., Zhou, Z., Wang, X., and Bi, X.: A review
754 of atmospheric aging of sea spray aerosols: Potential factors affecting chloride depletion, Atmos
755 Environ, 290https://doi.org/10.1016/j.atmosenv.2022.119365, 2022.
756 Su, B. J., Zhuo, Z. M., Fu, Y. Z., Sun, W., Chen, Y., Du, X. B., Yang, Y. X., Wu, S., Xie, Q. H., Huang,
757 F. G., Chen, D. H., Li, L., Zhang, G. H., Bi, X. H., and Zhou, Z.: Individual particle investigation
758 on the chloride depletion of inland transported sea spray aerosols during East Asian summer
759 monsoon, Sci Total Environ, 765https://doi.org/10.1016/j.scitotenv.2020.144290, 2021.
760 Sullivan, R. C., Moore, M. J. K., Petters, M. D., Kreidenweis, S. M., Roberts, G. C., and Prather, K. A.:
761 Timescale for hygroscopic conversion of calcite mineral particles through heterogeneous reaction
762 with nitric acid, Phys Chem Chem Phys, 11, 7826-7837, https://doi.org/10.1039/b904217b, 2009.
763 Tobo, Y., Adachi, K., DeMott, P. J., Hill, T. C. J., Hamilton, D. S., Mahowald, N. M., Nagatsuka, N.,
764 Ohata, S., Uetake, J., Kondo, Y., and Koike, M.: Glacially sourced dust as a potentially significant
765 source of ice nucleating particles, Nat Geosci, 12, 253-258, https://doi.org/10.1038/s41561-019-
766 0314-x, 2019.
767 Vancoppenolle, M., Meiners, K. M., Michel, C., Bopp, L., Brabant, F., Carnat, G., Delille, B., Lannuzel,
768 D., Madec, G., Moreau, S., Tison, J.-L., and van der Merwe, P.: Role of sea ice in global
769 biogeochemical cycles: emerging views and challenges, Quaternary Science Reviews, 79, 207-230,
770 https://doi.org/10.1016/j.quascirev.2013.04.011, 2013.
771 Verdugo, P.: Marine microgels, Annual Review of Marine Science, 4, 375-400,
772 https://doi.org/10.1146/annurev-marine-120709-142759, 2012.
773 Verdugo, P., Alldredge, A. L., Azam, F., Kirchman, D. L., Passow, U., and Santschi, P. H.: The oceanic
774 gel phase: a bridge in the DOM-POM continuum, Mar Chem, 92, 67-85,
775 https://doi.org/10.1016/j.marchem.2004.06.017, 2004.
776 Wang, Y. Q.: MeteoInfo: GIS software for meteorological data visualization and analysis, Meteorol.
777 Appl., 21, 360-368, https://doi.org/10.1002/met.1345, 2014.
778 Wang, Y. Q., Zhang, X. Y., and Draxler, R. R.: TrajStat: GIS-based software that uses various trajectory
779 statistical analysis methods to identify potential sources from long-term air pollution measurement
780 data, Environ Modell Softw, 24, 938-939, https://doi.org/10.1016/j.envsoft.2009.01.004, 2009.
781 Willis, M. D., Leaitch, W. R., and Abbatt, J. P. D.: Processes Controlling the Composition and
782 Abundance of Arctic Aerosol, Rev Geophys, 56, 621-671, https://doi.org/10.1029/2018rg000602,
783 2018.
784 Wilson, T. W., Ladino, L. A., Alpert, P. A., Breckels, M. N., Brooks, I. M., Browse, J., Burrows, S. M.,
785 Carslaw, K. S., Huffman, J. A., Judd, C., Kilthau, W. P., Mason, R. H., McFiggans, G., Miller, L.
786 A., Najera, J. J., Polishchuk, E., Rae, S., Schiller, C. L., Si, M., Temprado, J. V., Whale, T. F.,
787 Wong, J. P., Wurl, O., Yakobi-Hancock, J. D., Abbatt, J. P., Aller, J. Y., Bertram, A. K., Knopf, D.
788 A., and Murray, B. J.: A marine biogenic source of atmospheric ice-nucleating particles, Nature,
789 525, 234-238, https://doi.org/10.1038/nature14986, 2015.
790 Yan, J., Jung, J., Lin, Q., Zhang, M., Xu, S., and Zhao, S.: Effect of sea ice retreat on marine aerosol
791 emissions in the Southern Ocean, Antarctica, Sci Total Environ, 745, 140773,
792 https://doi.org/10.1016/j.scitotenv.2020.140773, 2020a.
793 Yan, J., Jung, J., Zhang, M., Xu, S., Lin, Q., Zhao, S., and Chen, L.: Significant Underestimation of
794 Gaseous Methanesulfonic Acid (MSA) over Southern Ocean, Environ Sci Technol, 53, 13064-

13070, https://doi.org/10.1021/acs.est.9b05362, 2019.
Yan, J., Jung, J., Zhang, M., Bianchi, F., Tham, Y., Xu, S., Lin, Q., Zhao, S., Li, L., and Chen, L.: Uptake selectivity of methanesulfonic acid (MSA) on fine particles over polynya regions of the Ross Sea, Antarctica, Atmos Chem Phys, 20, 3259-3271, https://doi.org/10.5194/acp-20-3259-2020, 2020b.
Yang, X., Pyle, J. A., and Cox, R. A.: Sea salt aerosol production and bromine release: Role of snow on sea ice, Geophys Res Lett, 35https://doi.org/10.1029/2008gl034536, 2008.
Young, L.-H., Li, C.-H., Lin, M.-Y., Hwang, B.-F., Hsu, H.-T., Chen, Y.-C., Jung, C.-R., Chen, K.-C., Cheng, D.-H., Wang, V.-S., Chiang, H.-C., and Tsai, P.-J.: Field performance of a semi-continuous monitor for ambient PM2.5 water-soluble inorganic ions and gases at a suburban site, Atmos Environ, 144, 376-388, https://doi.org/10.1016/j.atmosenv.2016.08.062, 2016.
Zawadowicz, M. A., Froyd, K. D., Murphy, D. M., and Cziczo, D. J.: Improved identification of primary biological aerosol particles using single-particle mass spectrometry, Atmos Chem Phys, 17, 7193-7212, https://doi.org/10.5194/acp-17-7193-2017, 2017.
Zhang, T., Fiamingo, M., and Allen, H. C.: Trace Metal Enrichment Driven by Phosphate Functional Group Binding Selectivity, Journal of Geophysical Research: Oceans, 123, 5286-5297, https://doi.org/10.1029/2018jc013926, 2018.